CHALLENGES AND LIMITATIONS FOR *IN SITU* PARTICLE TRACKING IN AVALANCHES

Robert Winkler[1], Jan-Thomas Fischer[2,], Peter Hergel[1], Michael Neuhauser[2], Betty Sovilla[3], Walter Steinkogler[4]

[1] *Department of Mechatronics, University of Innsbruck*
[2] *Department of Natural Hazards, Austrian Research Centre for Forests*
[3] *WSL Institute for Snow and Avalanche Research SLF*
[4] *Wyssen Avalanche Control*

ABSTRACT: A first approach to apply methods of inertial navigation for a motion tracking in a real-scale snow avalanche is presented. In the course of an artificially triggered avalanche event near the Flüelapass in Switzerland in January 2013, *in situ* inertial measurements (accelerations and angular velocities) have been combined with supplementary velocity measurements by means of Global Positioning System (GPS) and Doppler radar. Specifically, a commercial 9-axis Inertial Measurement Unit (IMU) has been mounted inside a rigid sphere and placed in the avalanche track such that it was entrained by the moving snow. To determine velocity and position, standard methods of state estimation (like Kalman filtering) are not optimally suited for this specific case. Instead, a new time integration algorithm is applied. The procedure turns out to be stable over a time period of about 4 s, which corresponds to a path length of about 65 m. The obtained velocity evolution fits well with the corresponding GPS and radar results. A comparison of the derived IMU trajectory with the corresponding topography reveals the reliability of position data within this time period. The spatial resolution of the IMU trajectory is such that a vertical motion of the sensor unit relatively to the terrain can be detected.

Keywords: Avalanche dynamics, motion tracking, inertial measurement unit, IMU, GPS, Doppler radar.

1. INTRODUCTION

An improved knowledge of internal avalanche dynamics is desirable not only from a theoretical point of view but also for a reliable prediction of impact pressures and of the transport of avalanche victims. During the past few years, several researchers have developed independently the idea to apply methods of inertial navigation for a motion tracking in gravitational mass movements (Fischer and Rammer, 2010; Vilajosana et al., 2011). In the context of snow avalanches the most promising real-scale experiment so far has been performed at the Flüelapass field site in Switzerland on January 23rd 2013 (Steinkogler et al., 2015), where infrared thermography measurements have been accompanied by Doppler radar (particle velocities) and inertial measurements (accelerations and angular velocities). In this contribution we discuss the evaluation of these inertial data with the supplementary Doppler radar, Global Positioning System (GPS) and terrestrial laser scanning measurements.

2. MEASUREMENT SET-UP

For the data acquisition, a commercial 9-axis Inertial Measurement Unit (IMU), consisting of accelerometers, gyroscopes, magnetometers, and a GPS receiver, has been integrated with a power supply and a data storage facility in a spherical, rigid housing. The housing properties are chosen to resemble a snow granule typically found in avalanche deposits (Bartelt and McArdell, 2009) with a density of $\approx$ 300 kg/m^3 and a diameter of $\approx$ 16 cm (Fischer and Rammer, 2010). The test site is located close to Davos, Switzerland [46.748621° (N), 9.945134° (E), WGS84]. The avalanche path is a north-east facing slope, with a vertical drop of 600 m. Deposits of larger avalanches typically reach a lake located at 2374 m a.s.l. at the bottom of the slope(Figure 1). The slope angle ranges from $50°$ in the rock face in the upper part to $20°$ at the beginning of the runout zone with an average of $30°$ of the open slope around 2600 m a.s.l. The avalanche had an approximate destructive size d2 (CAA, 2016) and was released artificially. Further details are available in Steinkogler et al. (2015). The avalanche entrained the motion sensor in the upper part of the open avalanche track. While the main body of the avalanche starved along the track, single snow granules, including the motion sensor, continued to travel to the bottom of the slope.

3. SUPPLEMENTARY MEASUREMENTS

GPS measurements in snow have several limitations. The main ones are shadowing effects in mountain environments and the signal attenuation due to

Figure 1: Map of the test site including the main avalanche deposit (blue) and the measured GPS coordinates of the sensor movement. Avalanche release, initial sensor location, stopping point of the main avalanche body, and the location of sensor deposition are marked.

the snow itself. For the presented avalanche experiment, seven visible satellites were available at the time of the measurement (Trimble Online Planing Tool©), such that start and end positions of the sensor unit could be obtained without major problems. However, during the avalanche movement a severe drift in the recorded GPS coordinates was observed, as long as the sensor travelled in the main avalanche body. Figure 1 shows the recorded GPS coordinates with a coordinate jump ($\approx$ 40 m in the horizontal direction) at the instant when the sensor left the main avalanche body and continued its path independently. The observed positioning error corresponds with results from static measurements in snow, which revealed positioning errors of up to 50 m (Schleppe and Lachapelle, 2006). Concerning the vertical accuracy, the GPS positions deviate up to $\approx$ 60 m from the terrain profile as long as the sensor is moving with the avalanche. A corrected trajectory was estimated from the measured GPS data in combination with terrestrial laser scanning data, which allows to deduce the corresponding velocities and which can be compared with results from the inertial measurements.

As a further velocity reference, we have evaluated material velocities in the head of the avalanche by means of Doppler radar measurements (see e.g. Neuhauser et al., 2018). To compare these velocities with IMU and GPS deduced velocities, they have been scaled with $1/\cos\delta$, where δ is the angle between the slope line and the radar beam (Fischer et al., 2016).

4. IMU DATA EVALUATION

In principle, IMUs are designed to enable the determination of angular orientation, translational velocity, and position. While the reliability of angular orientation is usually high, the one of velocity and, even more, of position suffer from an unavoidable drift. To obtain long-term stable results, additional information is required (GPS data, e.g.). The Flüela experiment has revealed that the sensor unit in action has been subjected to unexpected high and strongly varying rotation rates (with a maximum of about 200 rpm when travelling with the avalanche and twice as much in the subsequent rolling phase) and to frequent and randomly distributed acceleration peaks of up to 15 g ($\approx$ 150 m/s^2), compare Figures 2 and 3. In addition, the quality of recorded data is relatively low owing to the facts that no empirical experience has been available for an adequate design of the measurement set-up. These circumstances indicate that for the determination of velocity and position from the IMU data, standard methods of state estimation (nonlinear Kalman filter, e.g.) are prone to fail. State estimation relies on the assumption that the state of a physical system is basically determined by a dynamical model and subjected to stochastic disturbances. Regarding the rotational motion of the sensor unit driven by the avalanche, there is presently no concept from which an appropriate dynamical model could be derived. Considering the strongly, almost randomly, varying character of the raw data, it can be assumed that stochastic effects dominate the deterministic ones. Therefore, an alternative procedure for the evaluation of the avalanche data is proposed, which does *not* rely on a dynamical model:

1. The angular orientation of the sensor unit is determined via an adapted integration procedure applied to the gyrometer and magnetometer data
2. At each time step, the corresponding rotation matrix is employed to transform the measured data from the local sensor frame to the global one
3. Velocity and position data are obtained from the global acceleration components via standard time integration (trapezoidal rule)

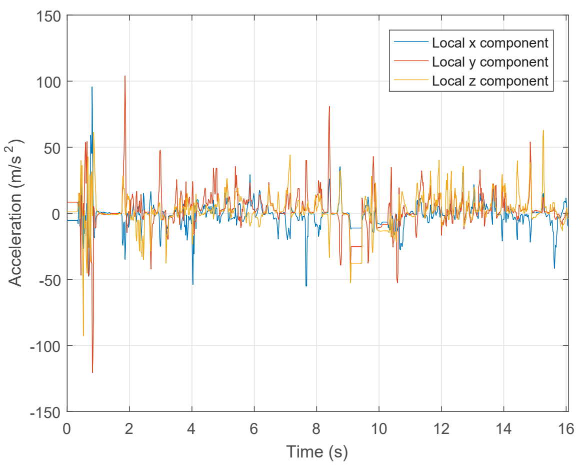

Figure 2: IMU acceleration components with respect to the corotating frame.

The integration of the gyrometer data deserves additional attention. As a basis, the kinematic differential equation governing the evolution of the rotation

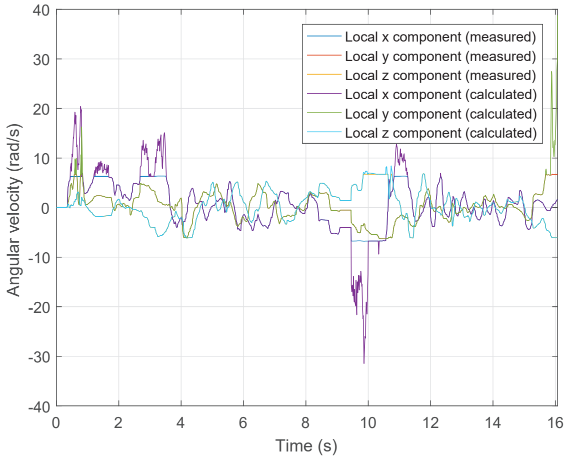

Figure 3: IMU angular velocity components with respect to the corotating frame. The raw data exhibit phases of sensor saturation, which can be bypassed by the new algorithm.

matrix $\mathbf{R}$ is taken,

$$\dot{\mathbf{R}} = \mathbf{R} \cdot {}^1\tilde{\omega} \tag{1}$$

with ${}^1\boldsymbol{\omega} = [\,{}^1\omega_1 \quad {}^1\omega_2 \quad {}^1\omega_3\,]^T$ being the vector of angular velocity components with respect to the corotating (i.e. sensor-fixed or local) frame, indicated by the left-hand superscript index 1 and ${}^1\tilde{\omega}$ the corresponding skew-symmetric 3×3 matrix. A well-known numerical integration scheme for (1) has been proposed by Hughes and Winget (1980)

$$\mathbf{R}_{n+1} = \mathbf{R}_n \cdot \left(\mathbf{I} + \frac{1}{2}\,\Delta t\,{}^1\tilde{\omega}^*_{n+\frac{1}{2}}\right) \cdot \left(\mathbf{I} - \frac{1}{2}\,\Delta t\,{}^1\tilde{\omega}^*_{n+\frac{1}{2}}\right) \tag{2}$$

by which means the orthogonality of $\mathbf{R}$ is preserved automatically. In (2), $\mathbf{I}$ is the 3×3 identity matrix and $\Delta t = t_{n+1} - t_n$ the time step. In the case of the classical Hughes-Winget algorithm,

$$ {}^1\omega^*_{n+\frac{1}{2}} = \frac{1}{2}\left({}^1\omega_n + {}^1\omega_{n+1}\right) \tag{3}$$

where ${}^1\omega^*_n$ and ${}^1\omega^*_{n+1}$ are the measured, corotational angular velocity components at the n-th and $(n+1)$-th time step, respectively. Here, an alternative procedure is proposed which takes into account additional information from the magnetometer data. The components of earth's magnetic field strength with respect to the global frame, ${}^0\mathbf{H}$, are virtually constant in time,

$$\mathbf{R} \cdot {}^1\mathbf{H} = {}^0\mathbf{H} = \mathrm{const} \tag{4}$$

That is, in particular,

$$\mathbf{R}_{n+1} \cdot {}^1\mathbf{H}_{n+1} = \mathbf{R}_n \cdot {}^1\mathbf{H}_n \tag{5}$$

Inserting (2) yields

$$\left(\mathbf{I} - \frac{1}{2}\,{}^1\tilde{\omega}^*_{n+\frac{1}{2}}\right)^{-1} \cdot {}^1\mathbf{H}_{n+1} = \left(\mathbf{I} + \frac{1}{2}\,{}^1\tilde{\omega}^*_{n+\frac{1}{2}}\right)^{-1} \cdot {}^1\mathbf{H}_n \tag{6}$$

Making use of the approximation $(\mathbf{I}+h\,\tilde{\omega})^{-1} \approx \mathbf{I}-h\,\tilde{\omega}$, which holds for sufficiently small parameters $h = \frac{1}{2}\,\Delta t$, a linear system of equations for the ${}^1\omega^*_{n+\frac{1}{2}}$ is obtained, which is, however, under-determined. Together with the condition (3), an over-determined system is obtained instead,

$$\begin{bmatrix} h\,\widetilde{({}^1\mathbf{H}_n + {}^1\mathbf{H}_{n+1})} \\ 2\,\mathbf{I} \end{bmatrix} \cdot {}^1\omega^*_{n+\frac{1}{2}} = \begin{bmatrix} {}^1\mathbf{H}_{n+1} - {}^1\mathbf{H}_n \\ {}^1\omega_n + {}^1\omega_{n+1} \end{bmatrix} \tag{7}$$

which can be solved for ${}^1\omega^*_{n+\frac{1}{2}}$ via the least squares method. The relative scaling of $\mathbf{H}$ and ω, having different physical units, refers to a weighting of conditions (6) and (3), respectively.

An additional benefit of the present approach is that it can easily handle missing data. The Flüela IMU data come along with the problem that the observed angular velocities occasionally exceeded the measurement range of the gyroscopes ($\pm 300°/\mathrm{s}$). At several instances only two out of the three ${}^1\omega_1$, ${}^1\omega_2$, ${}^1\omega_3$ are available (Figure 3). As long as there is at least one ω component available, the over-determined character of system is preserved and the integration algorithm works.

5. INERTIAL NAVIGATION RESULTS

By visual inspection, the following motion phases of the sensor unit can be identified from the IMU data:

1. Sensor unit at rest until time $t = 0$
2. Acceleration phase until time $t \approx 0.6\,\mathrm{s}$ (The sensor unit is entrained by the avalanche)
3. Ballistic phase (zero acceleration) until $t \approx 1.4\,\mathrm{s}$ (The sensor unit is saltating)
4. Impact at $t \approx 1.4\,\mathrm{s}$ (The sensor unit gets in contact with the snow again)
5. Acceleration signal is dominated by a basically random noise up to $t \approx 16\,\mathrm{s}$ and acceleration peaks indicate that some saltation takes place (The sensor unit is floating with the avalanche)
6. High spin rates until $t \approx 70\,\mathrm{s}$ (The sensor unit has left the avalanche and rolls downwards)
7. Sensor unit at rest for $t \gtrsim 70$ s

The most interesting time range referring to the avalanche motion is thus $[0, 16\,\mathrm{s}]$. Unfortunately, a failure of data recording has occurred at $t \approx 9\,\mathrm{s}$ such that no data are available for a time period of about $0.5\,\mathrm{s}$, which causes the time integration to fail.

The results of the procedure of Section 4 are presented in Figures 4 and 5. Figure 5 shows that the integration procedure is stable until $t \approx 4\,\mathrm{s}$ in the sense that condition (4) is fulfilled approximately, i.e. that the magnetic field strength is approximately constant. To initialize the time integration, the initial orientation of the sensor unit at rest is calculated from the direction of the magnetic field

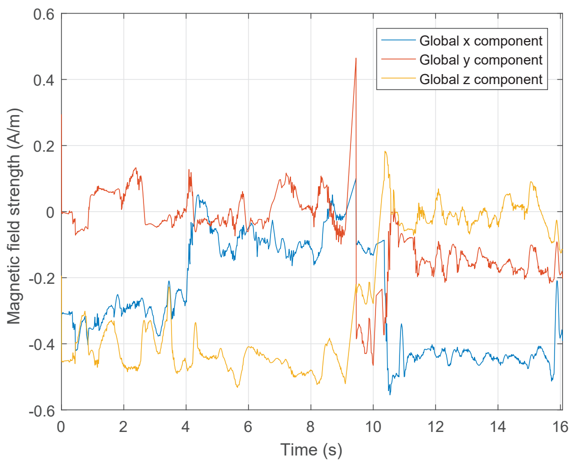

Figure 4: Magnetic field strength components with respect to the global frame (x = North, y = East, z = Down).

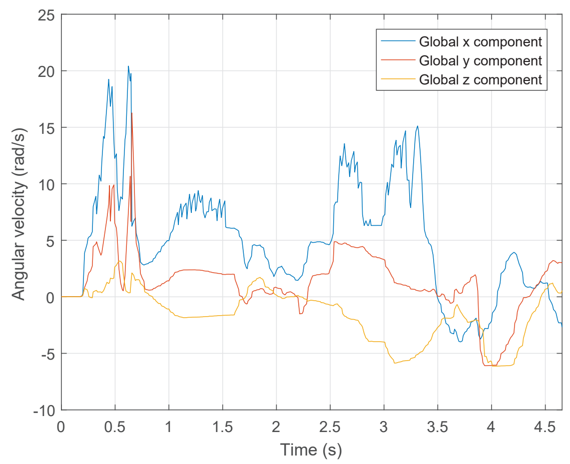

Figure 5: Angular velocity components with respect to the global frame (x = North, y = East, z = Down).

strength vector (whose horizontal projection indicates the northern direction = global x direction) and from the direction of the measured acceleration at rest (indicating the downward vertical direct = global z direction). The rotation matrix $\mathbf{R}_n$ at each time $t_n \in [0, 4\,\mathrm{s}]$ can be used to transform the measured quantities ${}^1\mathbf{H}_n$ (magnetic field strength), ${}^1\omega_n$ (angular velocity vector), and ${}^1\mathbf{a}_n$ (translational acceleration) to the global coordinate system, indicated by a left-hand superscript index 0,

$$
{}^0\mathbf{H}_n = \mathbf{R}_n \cdot {}^1\mathbf{H}_n\,, \qquad {}^0\omega_n = \mathbf{R}_n \cdot {}^1\omega_n \tag{8}
$$

$$
{}^0\mathbf{a}_n = \mathbf{R}_n \cdot {}^1\mathbf{a}_n - {}^0\mathbf{g} \tag{9}
$$

with ${}^0\mathbf{g}$ being earth's gravitational acceleration. Integrating the global accelerations by means of the trapezoidal rule, the velocity components ${}^0\mathbf{v}_n$ are obtained (Figure 7). The positions follow from an integration of velocities. The left-hand plot of Figure 8 draws the global z position versus the horizontal position $\sqrt{x^2 + y^2}$. The right-hand one shows the trajectory projected onto the horizontal x-y plane. In

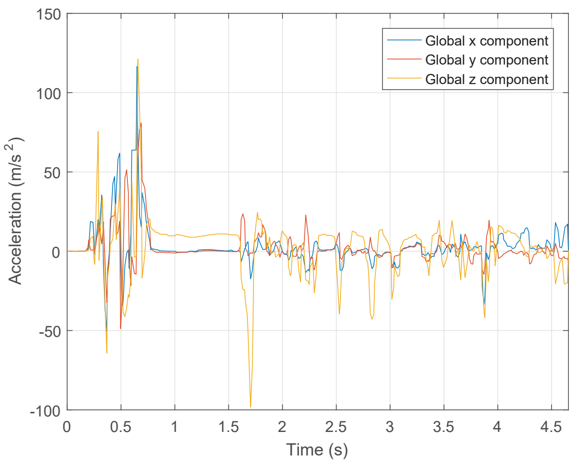

Figure 6: Acceleration components with respect to the global frame (x = North, y = East, z = Down).

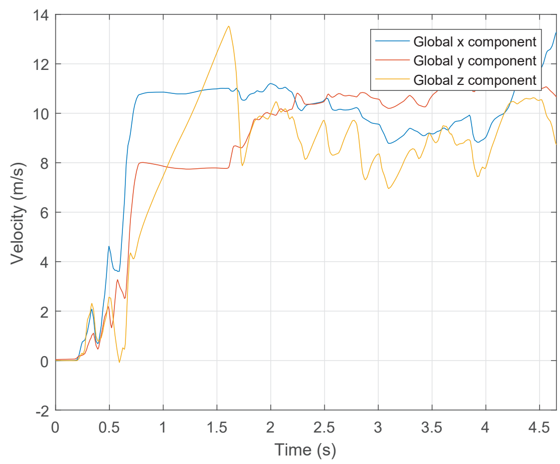

Figure 7: Velocity components with respect to the global frame (x = North, y = East, z = Down).

both plots the IMU results are compared with the GPS track (x and y coordinates) and the corresponding z coordinates obtained from the terrain model. As indicated in Section 3, the GPS positions have been manually corrected to match start and end positions as well as the terrain profile and are thus subjected to an uncertainty, which can hardly be quantified. It is emphasized that the evaluation of IMU positions and the one of GPS positions have been performed entirely independent of each other.

6. VELOCITY COMPARISON

Figure 9 shows the velocities obtained by the different measurement approaches. The main material velocities by means of Doppler radar measurements are not limited to the single sensor motion and include all avalanche and particle motion. The initial avalanche motion covers velocities, ranging between 15-25 m/s. When the avalanche entrains the motion sensor a rapid initial acceleration up to 15-

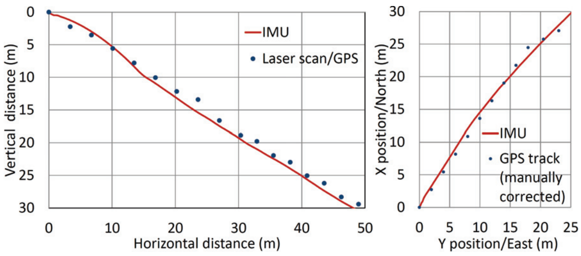

Figure 8: Vertical (z) position versus horizontal path length (left) and x-y trajectory (right). Note that GPS and IMU positions have been determined independently from each other.

20 m/s is observed for GPS and IMU velocities. The point, where the main avalanche stops is accompanied by a decrease in particle GPS velocities and the single particle motion is mainly below 5 m/s.

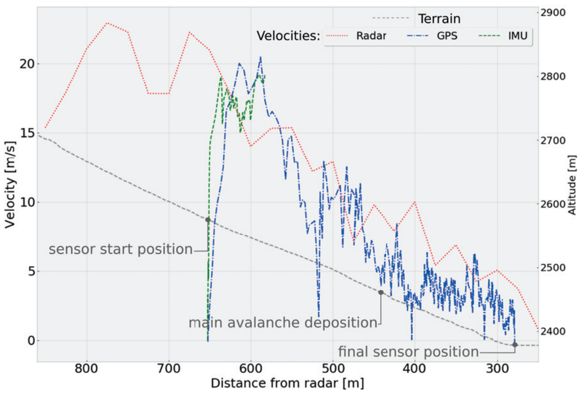

Figure 9: Velocities obtained by means of Doppler radar, GPS, and IMU measurements together with the terrain profile obtained from the terrestrial laser scan.

7. CONCLUSION

In situ measurements of a real scale avalanche trajectory utilizing an inertial navigation technique have been presented. In spite of several shortcomings coming along with the lack of any preceding experiences with the measurement set-up, it has been proven that the method is valid for the acquisition of qualitative and quantitative avalanche motion data. These are, in particular, the Lagrangian velocity and the trajectory of a single particle transported by the avalanche. The absolute positioning error is roughly estimated ~ 1 m over a travel distance of about 65 m and is rapidly growing afterwards. Within this range of reliability, the positioning error of the inertial navigation approach is definitely lower than the one of the GPS track (x, y) in combination with laser scanning data (z), (cf. Figure 8). It is emphasized that the accuracy of the evaluated trajectory is sufficiently high, such that a vertical motion relatively to the slope line can be detected. This can be seen from the pronounced saltation, which occurs as a result of the strong initial acceleration. Based on these first results, the authors are confident that the method can be developed further to provide an improved insight into the internal avalanche dynamics (segregation processes, e.g.). It is estimated that with a new generation of industrial grade (i.e. low cost) IMU sensors and with some improvements of the time integration procedure, a stable evaluation of velocity and position data is possible over a time period of at least 10 s and that a resolution on a sub-meter scale can be achieved, such that a vertical motion relatively to the terrain can be detected reliably. The capability of the inertial navigation approach could be raised strongly in combination with an additional, long-term stable positioning system such as terrestrial radio navigation (Erlacher et al., 2016, 2018). Finally, it is emphasized that future work on the topic must address the influence of size and shape of the sensor housing on the transport process.

REFERENCES

Bartelt, P. and McArdell, B. (2009). Instruments and Methods: Granulometric investigations of snow avalanches. *Journal of Glaciology*, 55(193):829–833.

CAA, C. A. A. (2016). Observation guidelines and recording standards for weather snowpack and avalanches. Technical report, Canadian Avalanche Association, Revelstoke, BC, Canada.

Erlacher, F., Dressler, F., and Fischer, J. (2018). First Experimental Insights on a Novel Sensor Network based Measurement Platform for Avalanche Dynamics. In *International Snow Science Workshop, Innsbruck, Austria - 2018*.

Erlacher, F., Weber, B., Fischer, J.-T., and Dressler, F. (2016). AvaRange - Using Sensor Network Ranging Techniques to Explore the Dynamics of Avalanches. In *12th IEEE/IFIP Conference on Wireless On demand Network Systems and Services (WONS 2016)*, pages 120–123, Cortina d'Ampezzo, Italy. IEEE.

Fischer, J. T., Köhler, A., Kofler, A., Sovilla, B., and McElwaine, J. (2016). Front and internal velocity distribution in powder snow avalanches. In *International Snow Science Workshop, Breckenridge, Colorado, USA - 2016*.

Fischer, J.-T. and Rammer, L. (2010). An introduction to inflow avalanche dynamics measurements using the SNOWBALL device. In *International Snow Science Workshop 2010, Squaw Valley, California USA*.

Hughes, T. J. R. and Winget, J. (1980). Finite rotation effects in numerical integration of rate constitutive equations arising in large-deformation analysis. *International Journal for Numerical Methods in Engineering*, 15:1862–1867.

Neuhauser, M., Kofler, A., Köhler, A., Schreiber, H., Gigele, T., Sovilla, B., Rammer, L., and Fischer, J. (2018). Avalanche Doppler radar monitoring - long term velocity measurements at Vallée de la Sionne. In *International Snow Science Workshop, Innsbruck, Austria - 2018*.

Schleppe, J. B. and Lachapelle, G. (2006). GPS Tracking Performance under Avalanche Deposited Snow. In *19th International Technical Meeting of the Satellite Division of The Institute of Navigation (ION GNSS 2006)*, pages 3105–3116, Fort Worth, TX.

Steinkogler, W., Sovilla, B., and Lehning, M. (2015). Thermal energy in dry snow avalanches. *The Cryosphere*, 9(5):1819–1830.

Vilajosana, I., Llosa, J., Schaefer, M., Surinach, E., and Vilajosana, X. (2011). Wireless sensors as a tool to explore avalanche internal dynamics: Experiments at the Weissflühjoch Snow Chute. *Cold Regions Science and Technology*, 65(2):242–250.